

## Irradiation-induced amorphization of graphite

Keisuke Niwase

*Department of Physics, Hyogo University of Teacher Education, Yashiro, Hyogo 673-14, Japan*

(Received 3 August 1994)

A model is proposed to explain the irradiation-induced amorphization of graphite. This model assumes that the single-vacancy concentration saturates to  $C_{VS}(T)$  at irradiation temperature  $T$ ; that the single-vacancy contained regions gradually transform to disordered regions, of which accumulation leads to amorphization; and that the transformation rate is proportional to the single-vacancy concentration. Utilizing  $C_{VS}(T)$  as a fitting parameter, this model explains the dose and the temperature dependencies of the Raman spectra of 25 keV  $\text{He}^+$ -irradiated highly oriented pyrolytic graphite. Also, the Arrhenius plot of the obtained values of  $C_{VS}^{-1}$ , which indicates the critical doses of amorphization, corresponds well to a previous TEM study, which showed two activation energies of 0.036 eV below  $\sim 573$  K and 0.25 eV above  $\sim 573$  K. By analyzing the chemical kinetics of the steady state, activation energies for single and di-interstitial migration of 0.14 and 0.86 eV, respectively, are obtained. The stored energy is attributed to a significant accumulation of di-interstitials below  $\sim 573$  K, which originated in the reduced annihilation with vacancies due to a barrier. By extending the theory to the quasisteady state with the collapsed line formation and the loop growth, the dimensional changes before amorphization can be also explained. This model should provide insight into the graphitization process and the formation mechanism of various carbon clusters.

### I. INTRODUCTION

The formation of lattice defects in solids under high-energy particle irradiations induce property changes and, in extreme cases, can lead to the loss of the long-range periodic order of the solids (amorphization). This type of irradiation-induced amorphization has been found in intermetallic compounds, ceramics, ordered alloys, ionic solids, etc.<sup>1-6</sup> Although a number of experiments and theoretical models has been attempted to clarify the amorphization mechanism, it is still not clear in terms of a defect-related process. Even for a simple solid such as Si it is unclear if amorphization occurs by quenching of an amorphous region produced by the collision cascade along a single ion track (heterogeneous formation) or by damage accumulation in the material until a critical threshold in the defect density is reached (homogeneous formation).<sup>7</sup>

Graphite, which amorphizes under irradiation,<sup>8-11</sup> is an ideal system to investigate the kinetic process of amorphization due to the presence of only carbon. However, a number of previous investigations on irradiated graphite, intended to study its usage as an atomic reactor material,<sup>12-16</sup> has revealed that graphite behaves in a complex manner under irradiation. This is attributed to two main reasons. First, the anisotropy of the graphite lattice requires a description of the motion of interstitials and vacancies in terms of activation energies parallel and perpendicular to the basal planes. For example, interstitial diffusion along the  $c$  axis is inhibited due to the very high activation energy of mobility required. Thus most of the interstitials which escape from the recombination of vacancies are considered to be reserved between the basal planes. Moreover, submicroscopic interstitial clusters consisting of  $4 \pm 2$  atoms<sup>17</sup> can move at rather low temperatures, but we have been unable to investigate the activation energy of mobility for these interstitial clusters. The activation energy of the mobility for vacancies, on the other

hand, is very high and it has been shown that the effect of the motion of vacancies in the basal planes does not appear below  $\sim 650$  °C.<sup>13,18</sup> Second, vacancy and interstitial clusters are believed to be unstable. Submicroscopic interstitial clusters may decompose to smaller ones and move around at rather low temperatures.<sup>19</sup> Also vacancy clusters may become a collapsed line of vacancy lattice sites, which are unable to recombine with interstitials.<sup>13,20,21</sup>

Recently, Raman spectroscopy has been widely used for the characterization of graphite<sup>22,23</sup> and investigations on the graphitization process<sup>24,25</sup> and on the change of graphite structure under irradiation.<sup>26-31</sup> The advantages of this method for the examination of graphite are a selective sensitivity to the structural changes in the basal plane, such as crystalline size<sup>22</sup> or the formation of a single vacancy or its clusters,<sup>29-31</sup> and extensive and continuous sensitivity over the range from ordered to amorphized graphite.<sup>8,27-31</sup> The present author and co-workers have been systematically investigating the defect structures and amorphization of graphite under 25 keV  $\text{D}^+$  and  $\text{He}^+$  irradiation or neutron irradiation by means of Raman spectroscopy and scanning and transmission electron microscopy (SEM, TEM).<sup>9,10,28,29,32,33</sup> We have shown that the effects of cascade and implanted species are negligibly small on the amorphization process of ion irradiation.<sup>9,32,33</sup> Therefore, we can discuss the amorphization mechanism as an homogeneous reaction of irradiation-produced defects.

In this paper, we will first review our previous experimental results on the changes of Raman spectra and the corresponding TEM diffraction patterns in Sec. II and discuss the relation between the defect formation and Raman spectra in Sec. III. Assuming a steady state with a saturation concentration of single vacancies, two models which can predict the Raman spectral changes will be presented; one is the single-vacancy-induced amorphization (SVIA) model and the other is the collapse-line- (divacancy-) induced amorphization

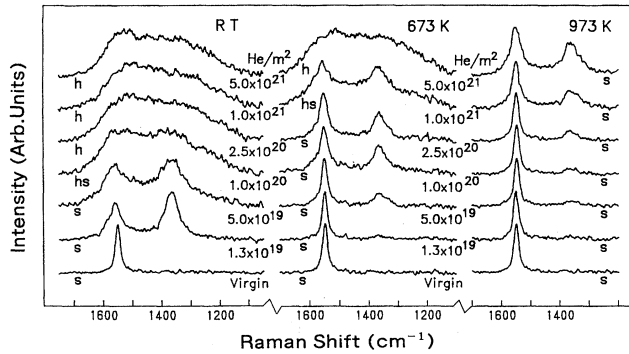


FIG. 1. Changes in the Raman spectra for HOPG foils irradiated with 25 keV  $\text{He}^+$  at three different temperatures: RT and 673 and 973 K. The appearance of the TEM diffraction pattern of the foils is denoted by *s* (spot), *hs* (halo and spot), and *h* (halo).

(CLIA) model. Both the models lead to the same conclusions, though they are completely different in terms of the detailed functions on the Raman spectral changes. Since we do not have theoretical and experimental models of a collapsed line, we will analyze the experimental results with the former model in Sec. IV and the latter model will be introduced in the Appendix. The changes of Raman spectra calculated by the model will be compared with the experimental results. The critical dose of amorphization predicted by the model will be also compared with the TEM result. It will be shown that the calculated results are in very good agreement with the experimental results.

Furthermore, analyzing the steady state with single and di-interstitials and single vacancies by chemical kinetics, the mobilities of single and di-interstitials will be estimated to be 0.14 and 0.86 eV, respectively. In Sec. V, the transformation mechanism from the crystalline to the amorphous phase, the stored energy, and the dimensional changes will be discussed. It will be shown that the dimensional changes can be explained by extending the theory from the steady state to the quasisteady state, taking the formation of interstitial loops and collapsed lines into account. It will be shown that a divacancy may transform into a collapsed line containing two five membered carbon rings, which are stable against approaches of interstitials. Finally, the mechanism of amorphization will be summarized. It will be demonstrated that most of the property changes of graphite under irradiation can be systematically explained by the present model.

## II. RAMAN SPECTRA AND TEM DIFFRACTION PATTERN OF 25 keV $\text{He}^+$ IRRADIATED GRAPHITE

Highly oriented pyrolytic graphite (HOPG) foils were irradiated with 25 keV  $\text{He}^+$  at temperatures ranging from room temperature (RT) to 973 K. The specimens were examined by means of transmission electron microscopy (TEM) and Raman spectroscopy. Details of experimental procedure have been explained elsewhere.<sup>28,29</sup>

Figure 1 compares the changes of Raman spectra of HOPG foils irradiated with 25 keV  $\text{He}^+$  at RT and 673 and 973 K. The spectrum before irradiation is given at the bottom of the figure, where the Raman active  $E_{2g}$  mode can only be found at  $1580\text{ cm}^{-1}$ . After irradiation, a new peak appears

around  $1355\text{ cm}^{-1}$ , which can be assigned as the maximum phonon density of states, caused by the relaxation of the wave-vector selection rule.<sup>34,35</sup> The appearance of the  $(10\bar{1}0)$  diffraction pattern has been investigated with TEM (Ref. 9) for each specimen and classified into three patterns of spot, halo and spot, and halo, which are referred as *s*, *hs*, and *h*, respectively in Fig. 1 and hereafter. One can see that the Raman spectral change closely correlates with the TEM diffraction change. The onset of amorphization denoted by *hs* corresponds to the onset of a remarkable increase of the two main Raman peaks, while the completion of amorphization denoted by *h* corresponds to a complete overlapping of the two peaks. Increasing the irradiation temperature is seen to delay the onset of the amorphization.

The Raman spectra are deconvoluted into several characteristic peaks with a least-squares algorithm. The spectra of the irradiated graphite denoted by *s* and *hs* are decomposed into four Lorentzian peaks: two dominant Lorentzian peaks at about  $1355$  and  $1580\text{ cm}^{-1}$  and additional two minor Lorentzian peaks at about  $1200$  and  $1500\text{ cm}^{-1}$ , while the spectra denoted by *h* cannot be fitted well by the Lorentzians, but can so by Gaussians.<sup>29</sup>

Figures 2(a) and 2(b) show the changes of the intensity ratio of the two peak ( $I_{1355}/I_{1580}$ ) and a full width at half maximum of the  $1580\text{ cm}^{-1}$  peak ( $\text{FWHM}_{1580}$ ), determined by the fitting analysis, against the dose. A difference can be clearly observed between the two. Below 473 K, the  $I_{1355}/I_{1580}$  is already larger than 1 at the initial stage of irradiation. After reaching a maximum, it gradually decreases and levels off at a value of  $\sim 0.9$ . Above 573 K, the  $I_{1355}/I_{1580}$  increases steadily and levels off at  $\sim 0.9$ . The amorphization corresponds to the dose range where the  $I_{1355}/I_{1580}$  levels off. On the other hand, the  $\text{FWHM}_{1580}$  gradually increases at the initial stage, but it increases dramatically when amorphization starts. The final stage of amorphization, denoted by *h*, corresponds to a value of  $\sim 180\text{ cm}^{-1}$ . Thus the change of the  $\text{FWHM}_{1580}$  more closely correlates with the amorphization process than that of the  $I_{1355}/I_{1580}$ .

Figure 3 shows how the  $\text{FWHM}_{1580}$  changes in relation to the dose, as the irradiated graphite becomes amorphous. Linear relationships can be seen at each irradiation temperature, but the increase rate decreases with increasing irradiation temperature. A significant reduction of the increase rate can be found between 573 and 673 K. Figure 4 shows the relation between the  $\text{FWHM}_{1580}$  and the  $I_{1355}/I_{1580}$  under 25 keV  $\text{He}^+$  irradiation. The three linear relations can be seen to correspond to the appearance of the TEM diffraction pattern of *s*, *hs*, and *h*. One should note, however, that several data below 473 K deviate from this relation, indicating different paths from the solid line to the dashed one.

## III. RAMAN SPECTRA AND IRRADIATION-PRODUCED DEFECTS

The intensity ratio of  $I_{1355}/I_{1580}$  for various grades of graphite has been accepted to have an inverse proportionality against a "crystalline size  $L_a$ ."<sup>22</sup> However, Niwase, Tanabe, and Tanaka have found a significant reduction of the  $I_{1355}/I_{1580}$  for RT-irradiated HOPG on annealing at 473 K, which cannot be explained by the crystalline size change.<sup>29</sup>

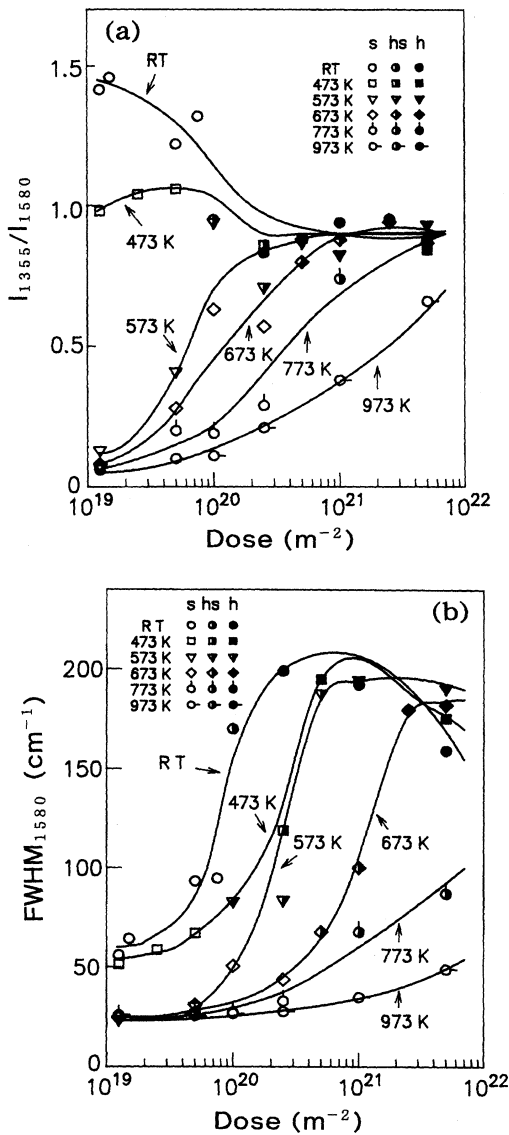


FIG. 2. (a) The intensity ratio of  $I_{1355}/I_{1580}$  and (b) the peak width of  $1580\text{ cm}^{-1}$  vs the dose in a logarithmic scale for HOPG foils irradiated with  $25\text{ keV He}^+$  at temperatures ranging from RT to  $973\text{ K}$ . The appearance of the TEM diffraction pattern of the foils is denoted by  $s$  (spot),  $hs$  (halo and spot), and  $h$  (halo). The solid curves are guides for eyes.

This reduction only occurred for unamorphized specimens, which correspond to the ones indicated by the solid line in Fig. 4. They have concluded that the change of the  $I_{1355}/I_{1580}$  under irradiation should not be attributed simply to the crystalline size change, but to defects produced in the basal planes such as single vacancies or vacancy clusters.<sup>29,33</sup> We will refer to the defects relating to the appearance of the sharp defect peak at  $1355\text{ cm}^{-1}$  as “in-plane defects” hereafter. Nakamura and Kitajima have found that the  $I_{1355}/I_{1580}$  is proportional to the square root of irradiation dose before amorphization.<sup>30</sup> They successfully explained this result as arising from the reduction of phonon correlation length due to vacancy formation. According to this model, an important

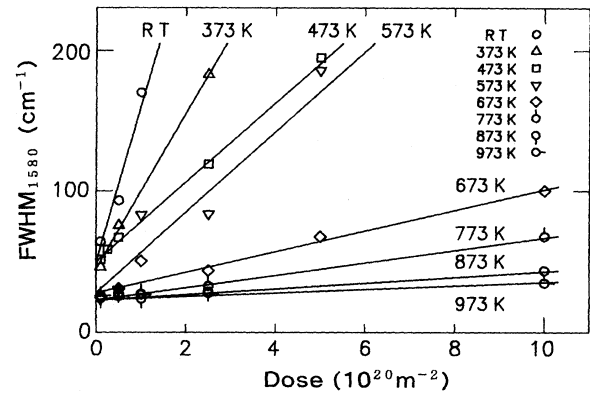


FIG. 3. Peak width of  $1580\text{ cm}^{-1}$  vs the dose in a linear scale for HOPG foils irradiated with  $25\text{ keV He}^+$  at temperatures ranging from RT to  $973\text{ K}$ . The dose range corresponds to the amorphizing stage. The peak widths are seen to linearly increase against the dose. The solid lines are guides for eyes.

relation between the atomic concentration of the in-plane defect  $C_V$  and the intensity ratio  $I_{1355}/I_{1580}$  has been found as

$$C_V = k(I_{1355}/I_{1580})^2, \quad (1)$$

where  $k$  is a constant. By replacing the  $C_V$  with  $C'_V = k^{-1}C_V$ , we get

$$C'_V = (I_{1355}/I_{1580})^2. \quad (2)$$

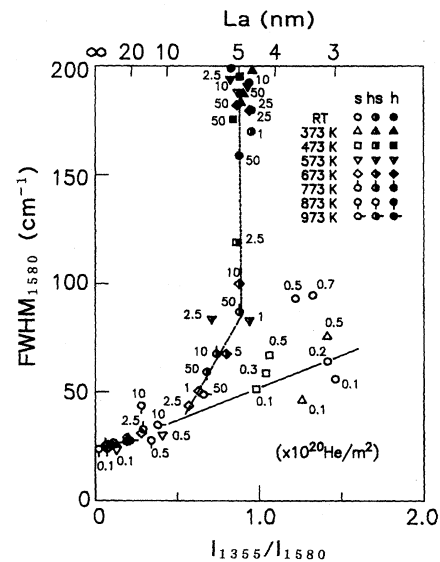


FIG. 4. Peak width of  $1580\text{ cm}^{-1}$  versus the intensity ratio of  $I_{1355}/I_{1580}$  for HOPG foils irradiated with  $25\text{ keV He}^+$  at temperatures ranging from RT to  $973\text{ K}$ . Open, half-solid, and solid symbols, respectively, correspond to the appearance of the TEM diffraction patterns of  $s$  (spot),  $hs$  (halo and spot), and  $h$  (halo). The in-plane crystalline size  $La$  calculated by Tuinstra and Koenig’s empirical relation (Ref. 22) is also indicated in the figure. The  $La$  should not be attributed to the in-plane crystalline size, but to the phonon correlation length broken by the in-plane defects, as described in the text.

We define the in-plane defect concentration  $C'_V$  expressed by the value of  $I_{1355}/I_{1580}$  as the one in Raman intensity units (R.I. units) and use it hereafter.

From Eq. (2), one can consider that the decrease in the value of the  $I_{1355}/I_{1580}$  at the point where it deviates from the solid line with increasing the irradiation temperature found in Fig. 4 corresponds to a decrease of the saturated concentration of in-plane defects, as mentioned in a previous paper.<sup>33</sup> Moreover, one can estimate the amount of in-plane defects which is repaired upon annealing. It has been shown that the intensity ratio, which reaches values of about 0.9 and 1.5, after 25 keV  $D^+$  irradiation at RT to doses of  $5.0 \times 10^{19}/\text{m}^2$  and  $1.0 \times 10^{20}/\text{m}^2$ , respectively, remarkably decreases on annealing at 473 K, and at 873 K finally reaches values of  $\sim 0.1$  and  $\sim 0.3$ , respectively.<sup>29</sup> From Eq. (2), it is estimated that 98% and 96% of the in-plane defect are recovered on annealing, respectively. This amount is incredibly large at such a low annealing temperature where vacancies are immobile. In general, most irradiated metals do not show such a significant recovery at vacancy-immobile temperatures since the amount of interstitial atoms which can annihilate with vacancies is less than 1% of the vacancies after irradiation due to an easy escape to specimen surfaces.<sup>36,37</sup> Thus we can conclude that a significant amount of interstitials, which is almost comparable with vacancies, remains in irradiated graphite as an unstable form before amorphization. This is probably due to the very high value of the activation energy on the migration of interstitials along the  $c$  axis, which inhibits them from passing across the basal planes.

After the onset of amorphization, the Raman spectra significantly broaden as shown in Fig. 1, suggesting the appearance of another defect relating to the amorphization. Niwase and Tanabe have investigated the relation between Raman spectra and defect structures by a combined study of Raman and high-resolution electron microscopy (HRTEM).<sup>33</sup> They have found little disorder in the lattice image except for the reduction of the contrast for unamorphized graphite when the corresponding Raman spectra show sharp features, supporting the above conclusion on the formation of in-plane defects which easily disappear on annealing. On the other hand, after the onset of amorphization the turbulence of the basal planes appeared when the corresponding Raman spectra significantly broadened. The defects found by the HRTEM image must be related to amorphization, and we will refer to them as “disordered regions” ( $D$  regions) hereafter. The  $D$  regions are stable on annealing at 873 K.<sup>29</sup> The concentration of the  $D$  regions may be expressed similarly to Eq. (1) as their existence would reduce the phonon correlation length. However, one should note that the intensity ratio gradually decreases with increasing the  $D$  regions below 473 K, as shown in Fig. 2(a), thereby indicating the weaker contribution from the  $D$  regions to the intensity ratio.

#### IV. THEORY AND COMPARISON WITH EXPERIMENT

##### A. Model on the change of Raman spectra (SVIA model)

The Raman intensity ratio of  $I_{1355}/I_{1580}$  and the peak width of the  $\text{FWHM}_{1580}$  give different information on the formation of the in-plane defects and  $D$  regions, as described

in the last section. The change of Raman spectra is now considered with the following assumptions.

(a) In-plane defects, detectable by Raman spectroscopy, are single vacancies and uncollapsed vacancy clusters. Single vacancies are saturated to the concentration of  $C_{VS}(T)$  at an irradiation temperature  $T$  to a dose  $t_1$ .

(b) Graphite structural regions with single vacancies ( $G$  regions) gradually transform into  $D$  regions. The transformation rate is proportional to the saturated concentration of single vacancies  $C_{VS}(T)$ . A detailed discussion of this assumption will be given in Sec. V A.

(c) The Raman intensity ratio ( $I_{1355}/I_{1580}$ ) and a peak width of  $1580 \text{ cm}^{-1}$  ( $\text{FWHM}_{1580}$ ) are expressed by the sum of Raman components from the  $G$  and  $D$  regions.

(d) The  $I_{1355}/I_{1580}$  has a square-root dependence on the concentration of the in-plane defect and  $D$  regions. The  $\text{FWHM}_{1580}$  has a square-root dependence on the concentration of the in-plane defects, but has a proportional dependence on the concentration of the  $D$  regions.

It should be noted that there is a clear difference in the definition between  $C_{VS}$  and  $C_V$ . The  $C_{VS}$  represents the saturated concentration of single vacancies in the  $G$  regions, while the  $C_V$  corresponds to the concentration of the in-plane defect in the total volume. Therefore, there may appear a case that the  $C_V$  becomes almost zero in spite of  $C_{VS}$  being a high value if the  $C_D$  becomes significantly higher than the  $C_V$ ; i.e., the graphite structure is highly amorphized.

According to (a) and (b), the concentration of the  $D$  regions,  $C_D$ , at a dose of  $t_2$  is given by

$$C_D(t_2) = k C_{VS}(T)(t_2 - t_1), \quad (3)$$

where  $k$  is a reaction constant. The value of  $C_D$ , formed before saturation of the in-plane defects, is negligibly small after several repetitions of  $t_1$ . From (c) and (d) the intensity ratio and the peak width of the  $1580 \text{ cm}^{-1}$  at  $t_2$  are, respectively, expressed as

$$I_{1355}/I_{1580}(t_2) = C_V(t_2)^{1/2} + A C_D(t_2)^{1/2}, \quad (4)$$

$$\text{FWHM}_{1580}(t_2) = E + B C_V(t_2)^{1/2} + D C_D(t_2), \quad (5)$$

where  $A$ ,  $B$ , and  $C$  are constant parameters and  $E$  is the peak width of virgin HOPG at room temperature. One should note that  $C_V$  and  $C_D$  are not expressed in atomic concentration, but in R.I. units, which are defined in the last section. From Eqs. (3)–(5), the  $\text{FWHM}_{1580}$  is expressed as

$$\begin{aligned} \text{FWHM}_{1580}(t_2) = & E + B [I_{1355}/I_{1580}(t_2) \\ & - A k^{1/2} C_{VS}(T)^{1/2} (t_2 - t_1)^{1/2}] \\ & + D k C_{VS}(T) (t_2 - t_1). \end{aligned} \quad (6)$$

##### B. Application of the model to the experimental results

Now, in comparing the model with the experimental results, it is clear that Eq. (6) cannot predict the changes of Raman spectra only by itself, as it contains three variable parameters of  $\text{FWHM}_{1580}(t_2)$ ,  $I_{1355}/I_{1580}(t_2)$ , and  $C_{VS}(T)$ . Then we use the experimental results of  $I_{1355}/I_{1580}$  [Fig. 2(a)] to give information on the changes of concentration of  $C_V$  and  $C_D$  under irradiation. All the constant parameters  $k$ ,  $A$ ,  $B$ ,  $D$ , and  $E$  can be definitely obtained from the experi-

mental results to be 0.2, 2/3, 30, 200, and 22, respectively. With these parameters and the experimental results of  $I_{1355}/I_{1580}$ , the model can predict the dose and temperature dependences of  $\text{FWHM}_{1580}$ , using the saturated concentration of single vacancies,  $C_{VS}(T)$ , in the  $G$  regions as a fitting parameter at each irradiation temperature. The procedures on the determination of the parameters and the fitting are explained in Appendix A. The results on the saturated concentration of  $C_{VS}$  and the saturation time  $t_1$  determined by the fitting analysis, the changes of the  $\text{FWHM}_{1580}$ ,  $C_V$  and  $C_D$  predicted by the model, and the experimental results of the  $I_{1355}/I_{1580}$  used in this calculation are summarized in Table I. The significant importance on the temperature dependence of the  $C_{VS}(T)$  obtained will be discussed in the following sections.

Figure 5 compares the experimental and predicted results of the dose dependence of the  $\text{FWHM}_{1580}$  at each irradiation temperature. Symbols represents the experimental results, while solid curves are the calculated results. The theoretical curves closely match the experimental results; the gradual increase of the  $\text{FWHM}_{1580}$  before amorphization and the remarkable increase after the onset of amorphization are well predicted. However, one should note that the present model is only applicable until the value of the  $\text{FWHM}_{1580}$  reaches  $\sim 200 \text{ cm}^{-1}$ , as shown in the figure. This is reasonable because the SVIA model is based on the graphite structure, before it is highly damaged. The effect of the increase of the  $D$  regions on the transformation will be discussed in Sec. V A. Figure 6 shows the relation between the  $\text{FWHM}_{1580}$  and the  $I_{1355}/I_{1580}$  as given by the calculation. By comparing with the experimental results shown in Fig. 4, one can find close correspondence between the model and experimental data, such as the detailed changes on the dose and temperature dependences. These very good predictions of the experimental results strongly support the present model.

Also, this model provides insight into the detailed changes of the concentrations of the in-plane defect  $C_V$  and  $D$  regions,  $C_D$ , as shown in Figs. 7(a) and 7(b). At RT,  $C_V$  decreases with increasing dose from the initial value of  $\sim 1.5$  and falls to zero at a dose of  $\sim 3 \times 10^{20} \text{ He/m}^2$ . A similar decrease of the  $C_V$  can be found for the irradiations at 373 and 473 K, though  $C_V$  remains almost constant during the initial stage of irradiation. Above 573 K, the trend changes:  $C_V$  at the initial dose is less than 0.2 and gradually increases to a certain value  $\sim 0.8$  at 573 K, for example, and then decreases. Thus changes of  $C_V$  can be clearly classified into two temperature ranges below 473 K and above 573 K. From the changes of the  $C_V$  and the  $C_D$ , we can clearly see that a decrease of  $C_V$  after the maximum is due to the transformation from the  $G$  regions to the  $D$  regions; the decrease of  $C_V$  in Fig. 7(a) corresponds to an increase of  $C_D$  when  $C_V$  becomes larger than  $\sim 0.5$ , as shown in Fig. 7(b).

Moreover, it should be noted that, although maximums of  $C_V$  below 673 K almost coincide with the saturated concentration of  $C_{VS}$ , corresponding to assumption (a) in Sec. IV A,  $C_V$  above 773 K is significantly higher than  $C_{VS}$ . From the definition of  $C_V$  and  $C_{VS}$  in this model, the value of  $(C_V - C_{VS})$  can be attributed to uncollapsed vacancy clusters. It has been shown that interstitial loops are decorated by a second population of smaller vacancy loops at 923 K,<sup>13</sup> suggesting a rather high mobility of vacancies. Thus one can

propose that vacancies begin to move at  $\sim 773 \text{ K}$ , resulting in the formation of clusters, which cannot transform to collapsed lines and are practically undetectable by a conventional electron microscope.

### C. Critical dose of amorphization and saturated concentration of single vacancies

Niwase *et al.* have investigated the temperature dependence of the critical dose of amorphization by the change of the TEM diffraction pattern.<sup>9,33</sup> They considered that the critical dose exists between the halo and spot pattern ( $hs$ ) and the halo pattern ( $h$ ) and found a significant change in the apparent activation energy from their Arrhenius plot.<sup>33</sup> In the present model, based on changes of the Raman spectra, we can clearly define the critical dose of amorphization ( $t_c$ ); that is, the dose at which the  $D$  regions reach a critical amount of  $A$ , thereby causing the disappearance of diffraction spots and the appearance of the halo in the TEM diffraction pattern of the irradiated graphite. Using Eq. (3) and neglecting the saturation time  $t_1$  since  $t_1 \ll t_c$  as shown in Table I, the amorphization condition can be expressed as

$$C_{VS}t_c = A', \quad (7)$$

where  $A'$  is  $k^{-1}A$ . This indicates that the critical dose of amorphization,  $t_c$ , is inversely proportional to the saturated concentration of single vacancies,  $C_{VS}$ .

Figure 8 shows the Arrhenius plot of the  $C_{VS}^{-1}$ , of which value is determined as the fitting parameter in the model calculation in the last section. We can find two linear relations, showing two activation energies of 0.036 eV below  $\sim 573 \text{ K}$  and of 0.25 eV above  $\sim 573 \text{ K}$ . These values will be discussed in the next section. It is interesting to compare the change of  $C_{VS}^{-1}$  with the TEM diffraction pattern on amorphization. Notably, two lines parallel to the Raman results can be drawn passing between the two points denoted by  $hs$  and  $h$  at each temperature, as shown in Fig. 8. The correlation of the temperature dependence of the critical dose of amorphization given by the two different methods strongly supports the present model of the changes of the Raman spectra.

### D. Analysis by chemical kinetics

Here we discuss the two activation energies found by the Arrhenius plot of the  $C_{VS}^{-1}$  in Fig. 8 by chemical kinetics with the following assumptions.

- (a) Vacancies exist only as singles and cannot move.
- (b) Interstitials exist as singles and in pairs. The former can move freely above RT, while the latter are immobile below  $\sim 573 \text{ K}$ , but mobile above  $\sim 573 \text{ K}$ . Both defects move only between the basal planes two dimensionally.
- (c) A collision of a di-interstitial with a single vacancy induces their annihilation, making a residual interstitial which instantaneously annihilates with a single vacancy.

It will be shown in Sec. V C that now we do not need to consider the existence of dislocation loops as sink effects in this analysis. Thus a variation of the single interstitial concentration of  $C_I$  is

TABLE I. Values of the  $\text{FWHM}_{1580}$ ,  $C_V^{1/2}$ , and  $C_D^{1/2}$  calculated with the present model using the  $C_{VS}$  as a fitting parameter and the experimental results of  $I_{1355}/I_{1580}$ . The values of  $C_V^{1/2}$ ,  $C_D^{1/2}$ , and  $C_{VS}$  are expressed in the R.I. Unit defined in Sec. III.

Irradiation temp. (K)	$t_1$ ( $10^{20}$ He/m $^2$ )	$t_2$ ( $10^{20}$ He/m $^2$ )	$C_{VS}$ (R.I. Unit)	$C_V^{1/2}$ (R.I. Unit)	$C_D^{1/2}$ (R.I. Unit)	$I_{1355}/I_{1580}$	$\text{FWHM}_{1580}$ (cm $^{-1}$ )
RT	0.0	0.1	0.0	1.460	0.000	1.46	65.8
	0.1	0.2	2.8	1.262	0.237	1.42	71.1
	0.1	0.5	2.8	0.904	0.473	1.22	93.9
	0.1	1.0	2.8	0.477	0.710	0.95	137.1
	0.1	2.5	2.8	0.057	1.159	0.83	292.5
373	0.0	0.1	0.0	1.260	0.000	1.26	59.8
	0.1	0.5	1.5	1.181	0.346	1.41	81.4
	0.1	2.5	1.5	0.324	0.849	0.89	175.7
473	0.0	0.1	0.0	0.980	0.000	0.98	51.4
	0.0	0.5	1.0	0.907	0.200	1.04	57.2
	0.7	1.0	1.0	0.871	0.283	1.06	64.1
	0.7	2.5	1.0	0.398	0.693	0.86	129.9
	0.7	5.0	1.0	0.220	0.990	0.88	224.6
573	0.0	0.1	0.0	0.130	0.000	0.13	25.9
	0.0	0.5	0.0	0.410	0.000	0.41	34.3
	0.7	1.0	0.7	0.803	0.205	0.94	54.5
	0.7	2.5	0.7	0.375	0.502	0.71	83.7
	0.7	5.0	0.7	0.353	0.776	0.87	153.0
673	0.7	10.0	0.7	0.069	1.141	0.83	284.5
	0.0	0.1	0.0	0.080	0.000	0.08	24.4
	0.0	0.5	0.0	0.280	0.000	0.28	30.4
	0.7	1.0	0.17	0.564	0.099	0.63	40.9
	0.7	2.5	0.17	0.408	0.244	0.57	46.1
	0.7	5.0	0.17	0.549	0.377	0.80	66.8
	0.7	10.0	0.17	0.511	0.554	0.88	98.7
773	0.7	25.0	0.17	0.343	0.895	0.94	192.7
	0.0	0.1	0.00	0.060	0.000	0.06	23.8
	0.0	0.5	0.00	0.200	0.000	0.20	28.0
	0.7	1.0	0.04	0.157	0.049	0.19	27.2
	0.7	2.5	0.04	0.210	0.120	0.29	31.2
873	0.7	10.0	0.04	0.558	0.273	0.74	53.6
	0.7	50.0	0.04	0.461	0.628	0.88	114.7
	0.0	0.1	0.000	0.070	0.000	0.07	24.1
	0.0	0.5	0.006	0.324	0.024	0.34	31.8
	0.7	1.0	0.012	0.082	0.027	0.10	24.6
973	0.7	2.5	0.012	0.146	0.066	0.19	27.2
	0.7	10.0	0.012	0.180	0.149	0.28	31.9
	0.7	50.0	0.012	0.451	0.344	0.68	59.2
	0.0	0.1	0.000	0.070	0.000	0.07	24.1
	0.0	0.5	0.000	0.100	0.000	0.10	25.0
973	0.7	1.0	0.006	0.097	0.019	0.11	25.0
	0.7	2.5	0.006	0.179	0.046	0.21	27.8
	0.7	10.0	0.006	0.310	0.106	0.38	33.5
	0.7	50.0	0.006	0.498	0.243	0.66	48.8

$$dC_I/dt = P - Z_1 M_I C_I C_V - 2Z_2 M_I C_I^2, \quad (8)$$

where  $P$  is the production rate of Frenkel pairs,  $M_I$  is the mobility of single interstitial atoms characterized by the migration activation energy  $E_m^I$  as  $\nu_1 \exp(-E_m^I/kT)$ , and  $Z$ 's are the site numbers of the spontaneous reaction of each process. The second term shows the mutual annihilation of

single interstitial atoms and vacancies. The third term is the formation of di-interstitials. At temperatures below  $\sim 573$  K, where di-interstitials are immobile, the corresponding variation of single vacancies is given by

$$dC_V/dt = P - Z_1 M_I C_I C_V - 2Q C_{2i} C_V, \quad (9)$$

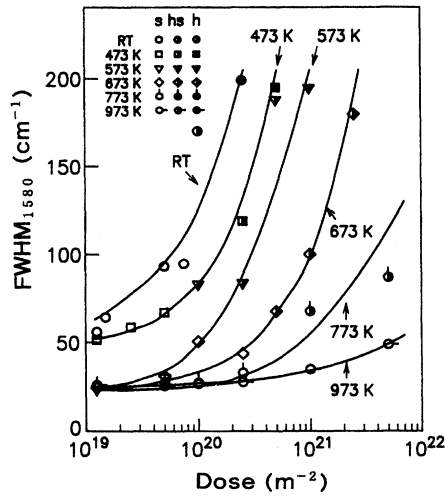


FIG. 5. Comparison of the peak width of  $1580 \text{ cm}^{-1}$  calculated by the present model with the experimental result. The calculated values are shown as solid curves.

where  $C_{2I}$  is the concentration of di-interstitials. The last term indicates the disappearance of di-interstitials with vacancies at a temperature-independent reaction rate  $Q$  when a di-interstitial and a single vacancy are formed within a spontaneous reaction region. A variation of di-interstitial concentration is shown by

$$dC_{2I}/dt = Z_2 M_I C_I^2 - Q C_{2I} C_V. \quad (10)$$

The total concentration of vacancies is equal to that of interstitials which have escaped from mutual recombination, as experimentally evidenced by the annealing experiment:

$$C_V = C_I + 2C_{2I}. \quad (11)$$

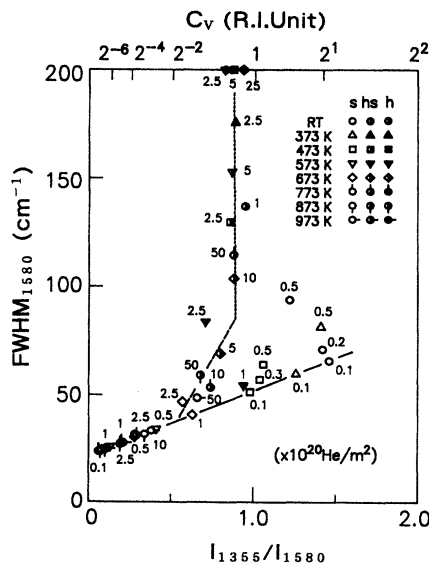


FIG. 6. Relation between the peak width of  $1580 \text{ cm}^{-1}$  and the intensity ratio of  $I_{1355}/I_{1580}$  predicted by the present model. The values of  $C_V$  are expressed in R.I. units defined in Sec. III.

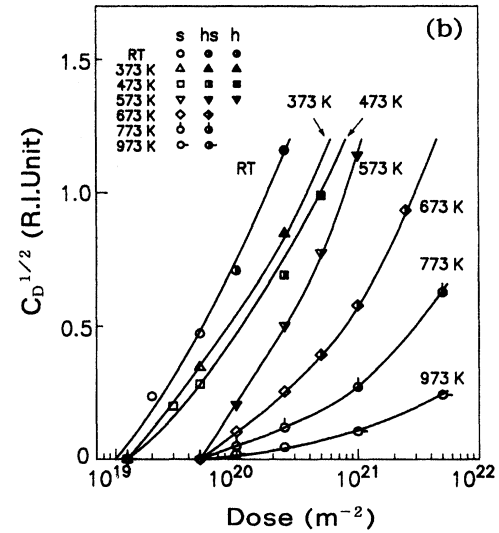
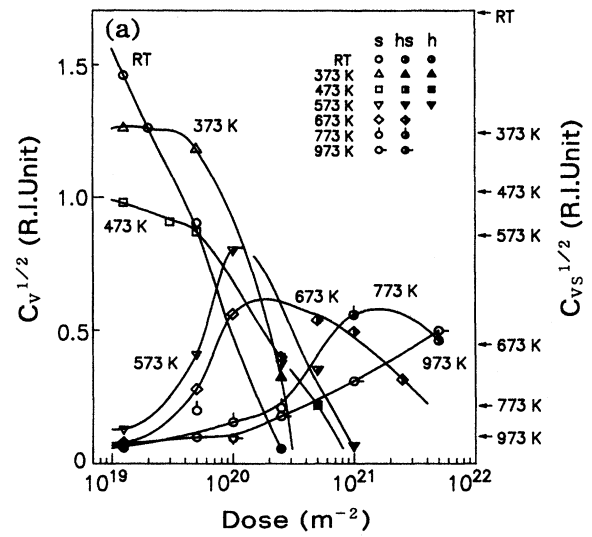


FIG. 7. Variations of the square root of the concentrations of (a) the in-plane defects,  $C_V^{1/2}$ , and (b) the  $D$  regions,  $C_D^{1/2}$ , given by the present model calculation. The square root of the saturated concentration of single vacancies,  $C_{VS}^{1/2}$ , at each irradiation temperature determined by the fitting analysis is shown in (a). The values of  $C_V^{1/2}$ ,  $C_D^{1/2}$ , and  $C_{VS}^{1/2}$  are expressed in R.I. units defined in Sec. III.  $C_V$  below  $673 \text{ K}$  remarkably decreases after saturating at the value  $\sim C_{VS}$  due to the transformation to the  $D$  regions, while  $C_V$  above  $773 \text{ K}$  becomes significantly higher than  $C_{VS}$ , indicating the formation of uncollapsed vacancy clusters.

At the steady state of irradiation when  $C_V$  reaches the saturation concentration of  $C_{VS}$ , Eqs. (8), (9), and (10) equal zero; we define these equations as Eqs. (8), (9), and (10), respectively. These relations lead to

$$Z_2 M_I C_I^2 = Q C_{2I} C_{VS}. \quad (12)$$

As  $Z_2 M_I \gg Q$  from (a) and (b), Eqs. (11) and (12) lead to  $C_{VS} > C_{2I} \gg C_I$ . Then Eq. (11) can be expressed as

$$C_{2I} \doteq C_{VS}/2. \quad (13)$$

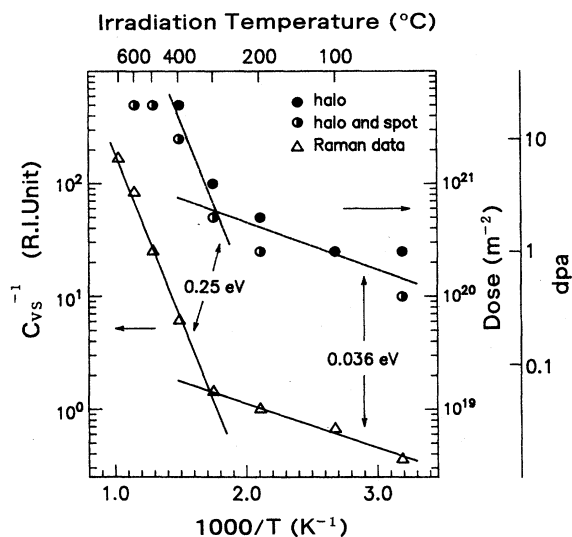


FIG. 8. Arrhenius plot of  $C_{VS}^{-1}$  determined by the fitting analysis. The values of  $C_{VS}^{-1}$  are expressed in R.I. units defined in Sec. III. This plot corresponds to the critical dose of amorphization as expressed by Eq. (7). Two linear relations are clearly seen, giving activation energies of 0.036 eV below  $\sim 573$  K and 0.25 eV above  $\sim 573$  K. Our previous TEM results on the change of diffraction pattern from halo and spot to halo (Ref. 33) can be seen to give two similar linear relations.

By substituting this relation into Eq. (12),  $C_I$  is given by

$$C_I = (2^{-1/2} Z_2^{-1/2}) C_{VS} Q^{1/2} M_I^{-1/2}. \quad (14)$$

As  $C_{VS} \gg C_I$ , Eq. (8) is approximated as

$$P - Z_1 M_I C_I C_{VS} \doteq 0. \quad (15)$$

By substituting Eq. (14) to Eq. (15), one can finally find the saturated concentration of single vacancies  $C_{VS}$ , as

$$C_{VS} = 2C_{2I} = (2^{1/4} Z_1^{-1/2} Z_2^{1/4}) P^{1/2} Q^{-1/4} M_I^{-1/4}. \quad (16)$$

At temperatures above  $\sim 573$  K where di-interstitials can move, one can deduce the  $C_{VS}$  by replacing the term of  $Q$  with  $Z_3 M_{2I}$ ,

$$C_{VS} = 2C_{2I} = (2^{1/4} Z_1^{-1/2} Z_2^{1/4} Z_3^{-1/4}) P^{1/2} M_I^{-1/4} M_{2I}^{-1/4}, \quad (17)$$

where  $M_{2I}$  is the jump frequency of di-interstitials characterized by their migration activation energy  $E_m^{2I}$  as  $\nu_2 \exp(-E_m^{2I}/kT)$ .

From Eqs. (16) and (17), it is found that the activation energies given below 573 K and above 573 K in Fig. 8 correspond to one-fourth of the migration energy of single interstitials and one-fourth of the sum of the migration energy of single and di-interstitials, respectively. Thus we have values of  $E_m^I = 0.14$  eV and  $E_m^{2I} = 0.86$  eV.

Also of interest is the significant difference in the values of the intercept at  $1/kT=0$  between the two lines in Fig. 8, which is about 2.4 in the logarithmic scale. According to the analysis given above, it corresponds to the difference in the coefficients between  $Q$  and  $Z_3 \nu_2$ , of which ratio is given as  $Q/Z_3 \nu_2 = 10^{-9.6}$ . Assuming that  $Z_3 \approx 10$  and  $\nu_2 \approx 10^{12}/s$ ,  $Q$  is

estimated to be about  $\sim 10^3/s$ . If the recombination were to occur at every vibrational frequency when a di-interstitial and a vacancy are formed in the reaction volume, i.e.,  $Q \approx Z_3 \nu_2$ , the values of the intercept at  $1/kT$  would be the same for the two lines in Fig. 8. Correspondingly, the concentration of di-interstitials below  $\sim 573$  K given by Eq. (16) would be about two orders of magnitude less than the real value. This implies that the very small value of the reaction rate of  $Q$  compared to the factor  $Z_3 \nu_2$  is the origin of the accumulation of di-interstitials, that is, the Wigner energy, thereby suggesting the existence of some barrier on the annihilation of di-interstitials and vacancies when di-interstitials are immobile.

## V. DISCUSSION

There are many reports suggesting that  $\sim 573$  K is a critical temperature where the properties of graphite drastically change: Stored energy is not important at irradiation temperatures above 573 K<sup>40</sup> the single-crystal expansion coefficient is changed by irradiation below  $\sim 573$  K<sup>16</sup> and the dose dependence of Young's modulus shows a very complex quality below  $\sim 573$  K.<sup>16</sup> As clearly shown in the last section,  $\sim 573$  K is a critical temperature where di-interstitials start to significantly decrease. This suggests that the above property changes closely to correlate with the accumulation of di-interstitials below  $\sim 573$  K. In this section, we discuss the transformation mechanism, the stored energy, the dimensional changes of graphite, and finally summarize the mechanism of amorphization and the property changes under irradiation.

### A. Transformation mechanism

The present model of the change of Raman spectra explains the experimental results, by assuming that the transformation rate from the  $G$  regions into the  $D$  regions is proportional to the single-vacancy concentration. The assumption implies that the transformation is a first-order reaction, like nuclear disintegration. However, a strict discussion of the self-collapsing process with this assumption does not lead to the dose dependence of the concentration of the  $D$  regions expressed in Eq. (3) without an additional factor as described in the following.

Let us consider the transformation from the  $G$  regions ( $C_C$ ) to the  $D$  regions ( $C_D$ ) with a transformation rate of  $k$ . The transformation is

$$-dC_C/dt = kC_C. \quad (18)$$

Taking an initial value of  $C_C = 1$  at  $t_0 = 0$ , the solution can be expressed as

$$C_C = \exp(-kt). \quad (19)$$

From the conservation relation of  $C_C + C_D = 1$ ,  $C_D$  is

$$C_D = 1 - \exp(-kt). \quad (20)$$

By replacing  $t' = kt$ , we can compare Eq. (3) with Eq. (20) as shown in Fig. 9. According to Eq. (20), the transformation rate from the  $G$  regions to the  $D$  regions gradually decreases with increasing dose due to the decrease in the total amount of  $G$  regions. However, as shown by a linear increase of the

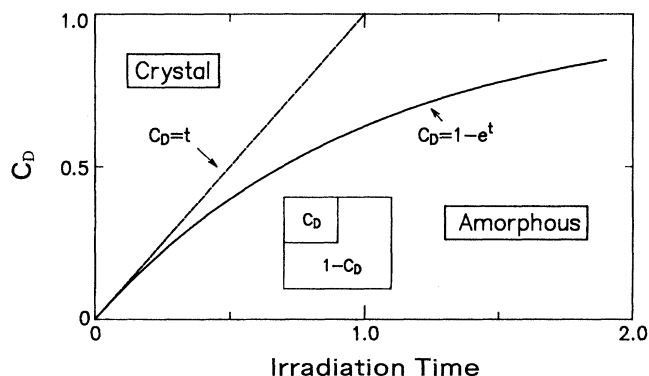


FIG. 9. Change of the concentration of the  $D$  regions,  $C_D$ , against the irradiation dose: (a) constant transformation rate expressed by Eq. (3); (b) a first-order reaction expressed by Eq. (20).

$\text{FWHM}_{1580}$  against the irradiation dose in Fig. 3, the constant transformation rate is experimentally supported. This means that some accelerating factor exists on the transformation, which increases as the number of  $D$  regions increases. One should remember that the transformation is not independent of the circumference, which is different from the case of nuclear disintegration.

We can suggest two possibilities as the circumference effect on the transformation of the  $G$  regions by the increase of the  $D$  regions: One is an energetical effect and the other is a kinetic effect. If the amorphization is assumed to occur in a localized region, in which the total energy  $E$  exceeds a critical value  $E_C$ ,  $E$  would be expressed not only by the defect concentration, but by the interface between the  $G$  and  $D$  regions. On the other hand, if the interface were to act as a preferential sink for interstitials, the vacancy concentration can increase after reaching  $C_{VS}$ , thereby accelerating the transformation rate. It should also be noted that the amorphization does not continue without irradiation, in spite of the existence of residual single vacancies in the matrix. This indicates that a mixing process of the position of fixed number of the saturated single vacancies under irradiation is important to the transformation and that the transformation occurs when the  $G$  regions realize a certain condition by chance sequences.

It is of interest to compare the amorphization process with the graphitization process. In both processes, vacancy plays a dominant role, but the result is completely opposite. The origin of the difference can be explained by the mobility of vacancies. When a vacancy is mobile, it acts to eliminate energetically high regions, i.e., disordered regions, thereby leading to graphitization. On the other hand, when a vacancy is immobile, random production of vacancies to the system such as irradiation at low temperatures makes the original structure unstable, which may induce transformation to disordered structures at a critical condition, eventually leading to amorphization. Recently, it has been found that graphite tubes or amorphous carbon are transformed under very intense and high-energy electron irradiation into an aggregate of fullerene clusters which are known as "bucky onions."<sup>38,39</sup> According to the present model, some effect must inhibit the transformation from the  $G$  regions to the  $D$

regions under these conditions. Further study on this phenomena may clarify the origin of the transformation.

### B. Stored energy

A characteristic phenomenon of neutron-irradiated graphite is striking release of the stored energy around 473 K, which is well known as the Wigner energy release. It has been shown that the stored energy release spectra behave in complex manners; the peak in the stored energy release rate at 473 K rises and then decreases with increasing dose; the rate at which energy is stored decreases with increasing irradiation temperature.<sup>18</sup> Several empirical relations, which can predict the behavior, have been proposed, but the relation between the stored energy and irradiation-produced defects is still not clear.

Judging from the significant value of the stored energy, we can easily guess that the stored energy relates to the recombination of interstitials and vacancies. As described in Sec. IV D, the single interstitial concentration is negligibly small compared to the di-interstitial concentration, and we can thus attribute the stored energy to the existence of di-interstitials and the corresponding vacancies. Accordingly, we may consider that the saturated concentration of di-interstitials expressed by Eqs. (16) and (17) is proportional to the maximum stored energy at each irradiation temperature. The temperature dependence of the maximum total stored energy can be found by viewing Fig. 8 upside down, as the total stored energy is proportional to the  $C_{VS}$ . It is clearly seen that the stored energy significantly decreases at  $\sim 573$  K, corresponding to the experimental results.<sup>40</sup> Moreover, the present model predicts that the total stored energy would decrease by further irradiation after the establishment of the steady state due to the transformation to the  $D$  regions, which is rather stable on annealing. We can find the corresponding decrease of the energy release rate of neutron-irradiated graphite with increasing the dose.<sup>41</sup>

One might guess that Eqs. (16) and (17) can give the activation energies of the mobility of both single interstitials and di-interstitials by measuring the temperature dependence of the maximum total stored energy. However, it is almost impossible in reality as it is not possible to measure the corresponding values due to the complicated process which releases the stored energy. The stored energy which we experimentally measure would be less than the values given in the equations due to absorption of di-interstitials by interstitial loops or the clustering process. However, the basic equations on the stored energy would be useful to analyze the process.

### C. Dimensional changes

Activation energies on the mobility of a single interstitial and a di-interstitial are given well by the present model as discussed so far. However, the model does not offer any possible explanation on the nonsaturation of the dimensional changes of the basal plane contraction and the elongation along the  $c$  axis observed in neutron-irradiated graphite before amorphization;<sup>41</sup> nor was there agreement with the observed interstitial loops which are a preferential sink for interstitials, since the present model only takes single vacancies and single and di-interstitials into account.

In order to explain the basal plane contraction, Kelly *et al.* have postulated that the collapsed lines are produced from linear vacancy groups in the basal plane.<sup>21</sup> The collapsed lines can grow only by displacements occurring close to their ends, followed by immediate collapse, but cannot recombine with interstitials. Kelly has explained the crystal dimensional changes with chemical kinetics using the above idea of the collapse of lines of vacant lattice sites and adapted the theory to high irradiation temperatures where vacancies can move in the basal plane.<sup>14</sup> He pointed out that the generation of submicroscopic interstitial clusters and their associated vacancies must be included to apply the theory at low temperatures. Lidiard and Perrin have also discussed the dimensional changes by the theory of loop growth with the model of collapsed vacancy lines.<sup>42</sup> They compared this theory to the crystal dimensional changes and electron microscope studies with a constant density of loops and demonstrated that agreement could only be obtained if the uniform single-vacancy concentration which annihilates with interstitials saturates rapidly. They also showed that to account for the lattice parameter changes at temperatures below 573 K, it was necessary to consider the presence of an equilibrium concentration of small interstitial groups.

We should note that both the former and latter authors have needed single vacancies and small interstitial groups to explain the experimental results of the dimensional changes. Specifically, the latter author's conclusion of the saturation of the two types of defects coincides with the assumptions used in the present model. In order to explain the dimensional change along the  $c$  axis and of the basal plane in the present model, we must give additional terms on the growth of interstitial loops and the production of the collapsed lines into the present simplified chemical kinetics. It would appear that these additional terms would change the present results completely; however, they do not with an assumption of a quasisteady state as explained in the following.

From the coincidence of the present model and Lidiard's conclusion, it is suggested that two balancing relations are established at the initial stage of irradiation,

$$\begin{aligned} T_I(\text{submicroscopic interstitial clusters}) \\ \approx T_V(\text{uncollapsed vacancies}) \end{aligned} \quad (21)$$

$$T_I(\text{interstitial loops}) \approx T_V(\text{collapsed lines}) \quad (22)$$

where  $T_I$  and  $T_V$  indicate the total concentration of interstitials and vacancies contained in the defect clusters shown within parentheses, respectively. We define the state with Eqs. (21) and (22) as the quasisteady state. The establishment of the quasisteady state can be found after a short period of irradiation in the detailed results calculated by Kelly *et al.*;<sup>21</sup> both the total concentrations of interstitials in the interstitial loops and the vacancies in the collapsed lines proportionally increase against the irradiation dose, maintaining equality. At the same time, the single-vacancy concentration is kept constant. The relations on the dimensional changes can be easily included in the present simplified equations only by adding the terms of the left- and right-hand sides of Eq. (22) to Eqs. (8) and (9), respectively. But further theoretical works are needed to clarify the reason why a quasisteady state is established under irradiation.

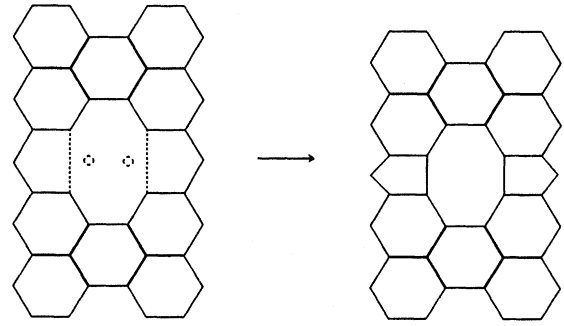


FIG. 10. Probable structure of the collapsed line formed from a divacancy. Note that the collapsed line contains two pentagons and one octagon. The collapsed line is stable against the approaches of single and di-interstitials.

In the quasisteady state, the production rate of the collapsed lines is given as  $dC_{NV}/dt = Z_4 C_{VS}^N$ , if the collapsed line were formed by  $N$  vacancies, where  $C_{NV}$  is the concentration of collapsed lines and  $Z_4$  is a geometrical factor, which is 3 when  $N=2$  for example. Using Eqs. (16) and (17), this is expressed as

$$dC_{NV}/dt = Z_4 (2^{1/4} Z_1^{-1/2} Z_2^{1/4})^N P^{N/2} Q^{-N/4} M_I^{-N/4} \quad (T < \sim 573 \text{ K}), \quad (23)$$

$$dC_{NV}/dt = Z_4 (2^{1/4} Z_1^{-1/2} Z_2^{1/4} Z_3^{-1/4})^N P^{N/2} M_I^{-N/4} M_{2I}^{-N/4} \quad (T > \sim 573 \text{ K}). \quad (24)$$

Correspondingly, the interstitial concentration contained in the interstitial loops proportionally increases against the dose at the rate of  $N$  times these relations. Then it can be concluded that Eqs. (23) and (24) correspond to the rate of the dimensional changes when the formation of the  $D$  regions is insignificant. According to this relation, the rate of dimensional changes is predicted to significantly decrease at  $\sim 573$  K, agreeing with the experimental results.<sup>14</sup> Moreover, the rate of dimensional changes is suggested to decrease with an increasing number of  $D$  regions, if the contribution to the dimensional changes from the  $D$  regions is insignificant. However, it has been shown that the turbulence of the basal planes due to the formation of the  $D$  regions may induce an elongation along the  $c$  axis.<sup>43</sup> This suggests that further work is required to quantitatively discuss this effect.

We can now compare the above relations to the experimental results. Schweitzer has shown the  $c$ -expansion rate ( $R_c$ ) of neutron-irradiated graphite and discussed it in terms of the mobility of interstitial.<sup>44</sup> From the Arrhenius plot of  $R_c$  given for irradiation temperatures from 30 to 180 °C, an activation energy of  $E_m^I$  of  $\sim 0.1$  eV can be calculated if  $N=2$ . By increasing  $N$ , the value of  $E_m^I$  becomes less than the value of 0.14 eV given in Sec. IV D, thereby indicating that the collapsed line is probably formed by the smallest vacancy cluster of divacancies.

Figure 10 shows a probable model of the transformation from a divacancy to a collapsed line. One should note that the collapsed line contains two pentagons and one octagon. To approve the present model on amorphization, the collapsed line must be stable against approaches of both the

single interstitials and di-interstitials. The ease of formation of a carbon-five ring and its stability in graphite structure may give important insight into this phenomenon, which is necessary to clarify the formation process of various carbon clusters, such as the fullerenes and graphite tubes.

There is little direct evidence of the existence of collapsed lines, but it is suggested that the appearance of a sharp halo ring in the (10 $\bar{1}$ 0) pattern of ion-irradiated HOPG at the onset of the amorphization<sup>9</sup> provides indirect evidence of collapsed lines. To make the sharp halo ring for the HOPG foil, a random rotation of the irradiated region around the *c* axis without introducing heavy disorder is necessary. Production of the collapsed line shown in Fig. 10 may induce randomly rotated graphite regions combined with the collapsed lines. Further insight into the problems of the amorphization of graphite can be found in the different results of He<sup>+</sup>- and D<sup>+</sup>-ion-irradiated HOPG given by Rutherford backscattering analysis (RBS).<sup>45,46</sup> The critical dose of the completion of amorphization judged by RBS was about 10 times smaller than the TEM results. Siegele, Roth, and Scherzer pointed out that displacement in the "two-dimensional" structure of graphite and a rearrangement of the surrounding carbon atoms could be the origin of the misjudgment of the critical dose by RBS.<sup>45</sup> Moreover, Ramos and Scherzer have indicated that changes in the damage profile did not occur below 600 K, but occurred instead above 720 K on annealing of a HOPG sample irradiated at 300 K with  $2 \times 10^{15}$  <sup>3</sup>He/cm<sup>2</sup>, which is considered to be before the onset of amorphization.<sup>46</sup> This result is quite different from the significant annealing effects observed at 473 K in the Raman spectra.<sup>29</sup> These differences imply that the defects relating to the Raman and RBS spectra are completely different: i.e., the former mainly relates to the uncollapsed vacancies shown in Eq. (21) while the latter mainly to the collapsed lines in Eq. (22). Therefore, a detailed comparison of the results given by the above two methods may clarify the development of the collapsed lines, which could not be directly detected by Raman spectroscopy.

#### D. Amorphization and the property changes of graphite

As described in the text, lattice defects formed under irradiation are roughly classified into three types of interstitial defects (single interstitials, di-interstitials, and interstitial loops), three types of vacancy defects (single vacancies, collapsed lines, and vacancy loops), and *D* regions. Figure 11 schematically shows the process of amorphization of graphite under irradiation, given by the present model calculations. The calculated results of the concentration of the in-plane defects,  $C_V$ , consisting of single vacancies and vacancy clusters shown in Fig. 7(a), are also indicated. The interstitial loops and collapsed lines, from which accumulations of these are responsible for the dimensional changes, are not indicated in the figure. Although the total number of interstitials contained in di-interstitials is almost equal to the total number of vacancies and the number of single interstitials is negligibly small as described in Sec. IV D, the ratio among these defects is not easily portrayed in the figure.

The process of amorphization shown in Fig. 11 and the property changes of irradiated graphite are summarized as follows. The concentrations of di-interstitials and the corresponding single vacancies gradually increase and reach a

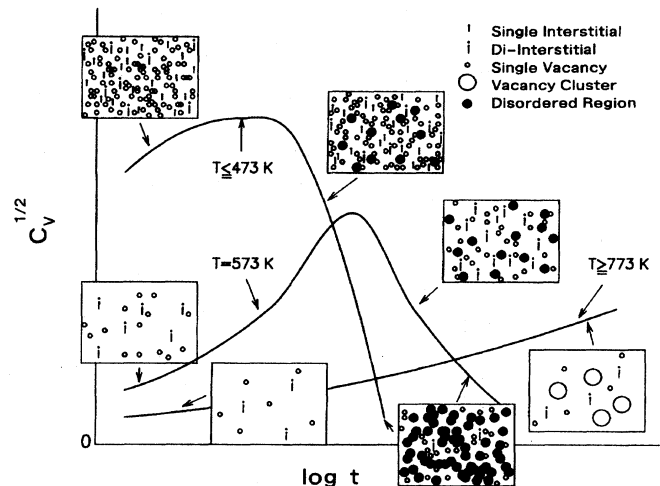


FIG. 11. Schematic representation of the change in defect distribution in irradiated graphite observed along the *c* axis. The variations of the concentration of the in-plane defects, given in Fig. 7(a), are shown by solid curves. The ratios between the densities of the different kinds of defects are ignored. The collapsed lines and interstitial loops relating to the dimensional changes before amorphization are not shown in the figure.

quasisteady state at a certain dose. The *G* regions can transform to the *D* regions under irradiation. The accumulation of the *D* regions eventually leads to amorphization. The transformation rate is proportional to the single-vacancy concentration. Below  $\sim 573$  K di-interstitials hardly move and there is an unknown barrier to their recombination with vacancies (Sec. IV D). Then di-interstitials and the corresponding single vacancies can accumulate to rather high concentrations. We concluded that this is the origin of the Wigner energy. Above  $\sim 573$  K, on the other hand, di-interstitials can freely move and easily recombine with vacancies, thereby resulting in little Wigner energy accumulation. The critical dose of amorphization is estimated to be inversely proportional to the saturated concentration of single vacancies and it significantly increases above  $\sim 573$  K. Vacancy clusters are formed after a long period of irradiation above  $\sim 773$  K, which can be seen as a gradual increase of  $C_V$ .

It should be noted that the formation of the *D* regions does not contribute to the property changes of irradiated graphite until the irradiation dose reaches a high enough order of magnitude, which can be estimated with  $C_{VS}$  using Eq. (3). This allows us to clearly divide the changes of graphite under irradiation into two stages: before and after the onset of amorphization in the logarithmic scale of dose as shown in Fig. 11. The former and latter stages correspond to the increasing and decreasing stages of  $C_V^{1/2}$ , respectively. The concentration of *D* regions falls in the range of 10–30 % after  $\sim 0.2$  displacement per atom (dpa) at room temperature and after  $\sim 20$  dpa at 773 K, which may be enough order to significantly affect the properties of graphite.<sup>9,10</sup> Thus we should discuss the property changes of graphite by dividing into the two stages of before and after the onset of amorphization.

Also it should be noted that a discrepancy still exists pertaining to the assignment of the two types of interstitials in

spite of a number of experimental works,<sup>12–14</sup> though the two activation energies of 0.14 and 0.86 eV obtained we have attributed to the migration energy for single and di-interstitials, respectively. Most authors treat the interstitials in a similar manner, but Iwata, Fujita, and Suzuki have assigned a value corresponding to the former di-interstitial, based on the theoretical estimation of a very small value of 0.016 eV for the migration energy for single interstitial atoms.<sup>47</sup> Moreover, Iwata found three activation energies of 1.34, 1.50, and 1.78 eV on the stored energy release spectra and attributed them to the activation energies for the decomposition of interstitial clusters consisting of di-interstitials.<sup>19</sup> The present results might be reconsidered with the idea of Iwata *et al.*, but it would be a more complicated one and more unknown factors would have to be introduced. We feel that more theoretical and experimental evidence is needed to support the idea of Iwata.

Of one concern in the present model is another possibility of the transformation mechanism. In the present model, the collapsed line is assumed to be undetectable by Raman spectroscopy due to its rather perfect structure and not related to amorphization. If it were detectable by Raman spectroscopy, the present model must be modified with a different assumption, that the formation of *D* regions originates from the existence of the collapsed lines in spite of the single vacancies (Appendix B). Correspondingly, the relation between the Raman spectra and irradiation-produced defects must be modified. Fortunately, the adapted model gives the same values for the saturated concentration of single vacancies,  $C_{VS}$ , and further modification on the latter discussion of the activation energies of migration of single interstitials and di-interstitials is not required. But to clarify the amorphization mechanism, it is important to know which is the origin for these results, single vacancies or the collapsed lines.

Moreover, though we have not discussed the chemical state of the irradiation-produced defects, Tanabe *et al.* have suggested that the in-plane defects may contain  $sp^3$  bonding.<sup>48</sup> As we described in Sec. IV D, the recombination between a di-interstitial and a single vacancy is not simple when di-interstitials are immobile. Also, a repulsive barrier  $U \sim 0.3$  eV between an interstitial and a single vacancy has been suggested by Goggin and Reynold.<sup>49</sup> Therefore, to clarify the mechanism of amorphization and the other property changes more basically, further investigations on the nature on the collapsed lines and single vacancies is needed.

In conclusion, the present model explains the amorphization process and property changes of irradiated graphite from an atomistic point of view. Moreover, the basic idea given by the model may be useful to clarify the graphitization process and the formation mechanism of fullerenes or other carbon clusters.

## VI. CONCLUSIONS

The Raman spectral changes and associated TEM diffraction changes of highly orientated pyrolytic graphite (HOPG) under 25 keV  $He^+$  irradiation have been systematically investigated in terms of irradiation dose and temperature. A model, based on the changes observed by Raman spectroscopy, has been proposed and compared with the experimental results. The mechanism of irradiation-induced amorphiza-

tion and the property changes have been discussed. The followings main conclusions have been reached.

(1) The Raman spectra of 25-keV  $He^+$ -irradiated HOPG, analyzed by a least-squares algorithm, show characteristic changes in the intensity ratio ( $I_{1355}/I_{1580}$ ) and a peak width of  $1580\text{ cm}^{-1}$  ( $FWHM_{1580}$ ). Before amorphization, there is a linear relation between the  $FWHM_{1580}$  and  $I_{1355}/I_{1580}$ . After the onset of amorphization, the data deviate from the linear relation and the value of  $I_{1355}/I_{1580}$ , at the deviation point, decreases with increasing irradiation temperature. The  $FWHM_{1580}$  proportionally increases against the dose, while the irradiated graphite is amorphizing, but the increase rate decreases with increasing temperature.

(2) A model of the changes of Raman spectra is given with the following assumptions: The single-vacancy concentration is saturated to  $C_{VS}$  in the initial stage of irradiation; single-vacancy-contained regions gradually transform to disordered regions, of which accumulation leads to amorphization; the transformation rate is proportional to the single-vacancy concentration. The dose and temperature dependences of the Raman spectra of  $He^+$ -irradiated HOPG can be accurately predicted by this model using the  $C_{VS}$  as a fitting parameter.

(3) The Arrhenius plot of the values of  $C_{VS}^{-1}$  given by the fitting, which is supposed to correspond to the critical doses of amorphization, corresponds to the one given by a previous TEM study, supporting the present model. The plot clearly shows two apparent activation energies of 0.036 eV below  $\sim 573$  K and 0.25 eV above  $\sim 573$  K.

(4) Analyzing the steady state with single and di-interstitials and single vacancies by chemical kinetics, the relation between  $C_{VS}$  and the mobilities of single and di-interstitials is deduced. We obtain the activation energies of migration for single and di-interstitials as 0.14 and 0.86 eV, respectively. Moreover, it is shown that some barrier exists on the recombination between di-interstitials and vacancies below  $\sim 573$  K where di-interstitials are immobile. This barrier is attributed to the origin of high accumulation of di-interstitials, i.e., of the stored energy.

(5) By extending the theory to the quasisteady state with the formation of collapsed lines and loop growth, the dimensional changes also can be quantitatively predicted. The analysis of the *c*-expansion rate by chemical kinetics indicates that divacancies would transform to a collapsed line. Uncollapsed vacancy clusters such as loops can be formed above  $\sim 773$  K, probably due to the vacancy mobility.

The present results can systematically explain the property changes of irradiated graphite in terms of irradiation-produced defects. Moreover, a basic knowledge of the defects in graphite given in the present study is useful to clarify the graphitization process and the formation mechanism of fullerene and related textures.

## ACKNOWLEDGMENTS

The author would like to express his gratitude to Professor T. Tanabe of Nagoya University, Professor Y. Miyamoto of Osaka University, Dr. I. Tanaka of Kyoto University, and Dr. H. Atsumi of Kinki University for valuable discussions. The Raman spectroscopy measurements were done at the Institute of Industrial Science of Osaka University.

### APPENDIX A: PROCEDURE OF CALCULATION

The detailed procedures of the calculation with the SVIA model are as follows.

(i) Find the constant parameters of  $A$ ,  $B$ , and  $E$  from the experimental results in Fig. 4. The parameters  $B$  and  $E$  are estimated to be 30 and 22 from the slope of the solid line and the intercept at the ordinate, respectively. The parameter  $A$  is estimated to be about 2/3 from the change of the value of  $I_{1355}/I_{1580}$  at RT when graphite amorphizes.

(ii) Find the saturated concentration of the in-plane defects,  $C_{VS}$  and the dose  $t_1$  for the RT result in Fig. 4. The value of  $C_{VS}^{1/2}$  is estimated to be about 1.5, but we used 1.67 ( $C_{VS}=2.8$ ), taking account of some annealing effect after irradiation.<sup>29</sup>

(iii) Find the constant parameters of  $k$  and  $D$ , which allow the best fit for the RT results. Judging from the nature of  $B$  and  $D$ , the value of  $D$  should be larger than that of  $B$ . The values used in the calculation are 0.2 and 200 for  $k$  and  $D$ , respectively. Though there is some flexibility in the choice of values of  $k$  and  $D$ , the product of  $kD$  must be about 40 to get a good fitting.

(iv) Find the values of  $C_{VS}$  and the corresponding  $t_1$ , which give the best fitting for each irradiation temperature.

It should be noted the value of  $C_{VS}$  at each irradiation temperature can be definitely obtained by the present model as the values of all the parameters except for  $C_{VS}$  in Eq. (6) are given experimentally.

### APPENDIX B: CLIA MODEL

Though the present model (SVIA model) explains the changes of Raman spectra of He<sup>+</sup>-irradiated HOPG, by assuming that the irradiation-induced amorphization originates from the creation of single vacancies, it must be modified if the collapsed lines are detectable by Raman spectroscopy. Here we introduce the collapsed-line-induced amorphization model (CLIA model) with the following assumptions.

(a) The single-vacancy concentration is saturated to  $C_{VS}(T)$  at a dose of  $t_1$  at an irradiation temperature of  $T$ . All divacancies transform to the collapsed lines.

(b) The collapsed-line-containing regions gradually transform to the  $D$  regions. The transformation rate is proportional to the concentration of collapsed lines,  $C_{2V}$ .

(c) The Raman intensity of  $I_{1355}/I_{1580}$  and the peak width of the FWHM<sub>1580</sub> are expressed by the sum of Raman components consisting of the collapsed lines and  $D$  regions.

(d) The FWHM<sub>1580</sub> has a square-root dependence on the concentration of the collapsed lines and  $D$  regions.

As the production rate of the collapsed lines is given by  $dC_{2V}/dt=Z_4C_{VS}^2$ , its concentration at a dose of  $t_2$  is expressed as

$$C_{2V}=Z_4C_{VS}^2(t_2-t_1), \quad (\text{B1})$$

where the amount of the collapsed lines formed before  $t_1$  is neglected. The linear increase of  $C_{2V}$  against irradiation dose corresponds well to the result given by Kelly *et al.*<sup>21</sup> According to (a) and (b), the concentration of the disordered regions  $C_D$  is given by

$$C_D(t_2)=2^{-1}kZ_4C_{VS}(T)^2(t_2-t_1)^2, \quad (\text{B2})$$

where  $k$  is a reaction constant. From (c) and (d) the intensity ratio ( $I_{1355}/I_{1580}$ ) and a peak width of 1580 cm<sup>-1</sup> (FWHM<sub>1580</sub>) are, respectively, expressed as

$$I_{1355}/I_{1580}(t_2)=C_V(t_2)^{1/2}+AC_D(t_2)^{1/2}, \quad (\text{B3})$$

$$\text{FWHM}_{1580}(t_2)=E+BC_V(t_2)^{1/2}+DC_D(t_2)^{1/2}, \quad (\text{B4})$$

where  $A$  shows the difference of the increase rate of  $I_{1355}/I_{1580}$  between the collapsed lines and  $D$  regions;  $B$  and  $D$  show the increase rates of the peak width for the collapsed lines and  $D$  regions, respectively; and  $E$  is the peak width of the virgin HOPG at room temperature. From Eqs. (B2)–(B4), the FWHM<sub>1580</sub> is expressed as

$$\begin{aligned} \text{FWHM}_{1580}(t_2) &= E + BI_{1355}/I_{1580}(t_2) + (D - AB) \\ &\quad \times (2^{-1}kZ_4)^{1/2}C_{VS}(T)(t_2 - t_1). \end{aligned} \quad (\text{B5})$$

It should be noted that this relation is similar to Eq. (6) given by the SVIA model in terms of the relation between  $C_{VS}(T)$  and  $t_2 - t_1$ . We can compare this model to the experimental results, using the same process given in Sec. IV B. Using constant parameters of  $A$ ,  $B$ ,  $D$ , and  $E$  as 2/3, 30, 230, and 22, respectively, and the value of  $2^{-1}kZ_4$  as 0.04, we can explain the dose and temperature dependence of the FWHM<sub>1580</sub>. Interestingly, the values of  $C_{VS}(T)$  determined by fitting trials almost coincide with the ones given by the SVIA model. Therefore, the latter discussions of the values of the activation energy of migration of single interstitials and di-interstitials, the stored energy, and the dimensional changes except for the critical dose of amorphization are the same with the CLIA model.

Here we discuss the critical dose of amorphization by the CLIA model. By defining the critical dose of amorphization,  $t_C$ , as the dose at which the amount of  $D$  regions reaches a critical amount of  $A$ , similarly as in Sec. IV C, the amorphization condition deduced with Eq. (B2) is

$$C_{VS}(T)t_C=A', \quad (\text{B6})$$

where  $A'=(2k^{-1}Z_4^{-1A})^{1/2}$  and  $t_C \gg t_1$ . One should note that this relation is the same as Eq. (7). Therefore, the modified model also gives the same conclusion on the critical dose of amorphization.

Thus the CLIA model leads to the same conclusions as the SVIA model. However, the two models are completely different in explaining the Raman spectral change and the amorphization process. The coincidence comes from the difference in the assumption of the relation between the FWHM<sub>1580</sub> and  $C_D$ . Further theoretical and experimental studies on the relation are awaited to judge the amorphization mechanism.

- <sup>1</sup>E. M. Schulson, *J. Nucl. Mater.* **83**, 239 (1979).
- <sup>2</sup>H. Mori, H. Fujita, M. Tendo, and M. Fujita, *Scr. Met.* **18**, 783 (1984).
- <sup>3</sup>H. Fujita, *Ultramicroscopy* **39**, 369 (1991).
- <sup>4</sup>M. Nastasi and J. W. Mayer, *Mater. Sci. Rep.* **6**, 1 (1991).
- <sup>5</sup>S. U. Campisano, S. Coffa, V. Raineri, F. Priolo, and E. Rimini, *Nucl. Instrum. Methods B* **80/81**, 514 (1993).
- <sup>6</sup>L. W. Hobbs, *Nucl. Instrum. Methods B* **91**, 30 (1994).
- <sup>7</sup>S. U. Campisano, S. Coffa, V. Raineri, F. Priolo, and E. Rimini, *Nucl. Instrum. Methods B* **80/81**, 514 (1993).
- <sup>8</sup>B. S. Elman, M. S. Dresselhaus, G. Dresselhaus, E. W. Maby, and H. Mazurek, *Phys. Rev.* **24**, 1027 (1981).
- <sup>9</sup>K. Niwase, M. Sugimoto, T. Tanabe, and F. E. Fujita, *J. Nucl. Mater.* **155–157**, 303 (1988).
- <sup>10</sup>K. Niwase and T. Tanabe, *J. Nucl. Mater.* **179–181**, 218 (1991).
- <sup>11</sup>K. Nakai, C. Kinoshita, and A. Matsunaga, *Ultramicroscopy* **39**, 361 (1991).
- <sup>12</sup>W. N. Reynolds, in *Radiation Damage in Graphite* (Pergamon, New York, 1965), p. 1.
- <sup>13</sup>R. A. Throver, in *Chemistry and Physics of Carbon*, edited by P. L. Walker, Jr. (Dekker, New York, 1969), Vol. 5, p. 217.
- <sup>14</sup>B. T. Kelly, *Physics of Graphite* (Applied Science, London, 1981).
- <sup>15</sup>A. Miyahara and T. Tanabe, *J. Nucl. Mater.* **155–157**, 49 (1988).
- <sup>16</sup>B. T. Kelly, *Materials Science and Technology* (VCH, New York, 1994), Vol. 10A, p. 366.
- <sup>17</sup>D. G. Martin and R. W. Henson, *Philos. Mag.* **9**, 659 (1964).
- <sup>18</sup>L. Binkele, *J. Non-Equilib. Thermodyn.* **3**, 257 (1978).
- <sup>19</sup>T. Iwata, *J. Nucl. Mater.* **133&134**, 361 (1985).
- <sup>20</sup>G. K. Williamson and P. Horner, *J. Br. Nucl. Energy Soc.* **3**, 269 (1964).
- <sup>21</sup>B. T. Kelly, W. H. Martin, A. M. Price, and J. T. Bland, *Philos. Mag.* **14**, 343 (1966).
- <sup>22</sup>F. Tuinstra and J. L. Koenig, *J. Chem. Phys.* **53**, 1126 (1979).
- <sup>23</sup>T. Tanabe, K. Niwase, N. Tsukuda, and E. Kuramoto, *J. Nucl. Mater.* **191–194**, 330 (1992).
- <sup>24</sup>R. O. Dillon, J. A. Woollam, and V. Katkanant, *Phys. Rev. B* **29**, 3482 (1984).
- <sup>25</sup>J. N. Rouzaud, A. Oberlin, and C. Beny-Bassez, *Thin Solid Films* **105**, 75 (1983).
- <sup>26</sup>M. S. Dresselhaus and R. Kalish, *Ion Implantation in Diamond, Graphite and Related Materials* (Springer-Verlag, Berlin, 1992).
- <sup>27</sup>B. S. Elman, M. Shayegan, M. S. Dresselhaus, H. Mazurek, and G. Dresselhaus, *Phys. Rev. B* **25**, 4142 (1982).
- <sup>28</sup>K. Niwase, K. Nakamura, I. Tanaka, Y. Miyamoto, and T. Tanabe, *J. Nucl. Mater.* **179–181**, 214 (1991).
- <sup>29</sup>K. Niwase, T. Tanabe, and I. Tanaka, *J. Nucl. Mater.* **191–194**, 335 (1992).
- <sup>30</sup>K. Nakamura and M. Kitajima, *Phys. Rev. B* **45**, 78 (1992).
- <sup>31</sup>E. Asari, M. Kitajima, and K. G. Nakamura, *Phys. Rev. B* **47**, 11 143 (1993).
- <sup>32</sup>K. Niwase, T. Tanabe, M. Sugimoto, and F. E. Fujita, *J. Nucl. Mater.* **168**, 191 (1989).
- <sup>33</sup>K. Niwase and T. Tanabe, *Mater. Trans. Jpn. Inst. Met.* **34**, 1111 (1993).
- <sup>34</sup>R. J. Nemanich and S. A. Solin, *Phys. Rev. B* **29**, 392 (1979).
- <sup>35</sup>P. Lespade, R. AL-Jishi, and M. S. Dresselhaus, *Carbon* **20**, 427 (1982).
- <sup>36</sup>N. Yoshida, M. Kiritani, and F. E. Fujita, *J. Phys. Soc. Jpn.* **39**, 86 (1975).
- <sup>37</sup>M. Kiritani, *Progress in the Study of Point Defects* (University of Tokyo Press, Tokyo, 1977), p. 247.
- <sup>38</sup>D. Ugarte, *Chem. Phys. Lett.* **207**, 473 (1993).
- <sup>39</sup>F. Banhart, *Philos. Mag. Lett.* **69**, 45 (1993).
- <sup>40</sup>J. C. Bell, H. Bridge, A. H. Cottrell, G. B. Greenough, J. H. Simmons, and W. N. Reynold, *Philos. Trans. R. Soc. London A* **254**, 361 (1962).
- <sup>41</sup>B. T. Kelly, W. H. Martin, and P. T. Nettle, *Philos. Trans. R. Soc. London A* **260**, 37 (1966).
- <sup>42</sup>A. B. Lidiard and R. Perrin, *Philos. Mag.* **14**, 433 (1966).
- <sup>43</sup>T. Tanabe, S. Muto, and K. Niwase, *Appl. Phys. Lett.* **61**, 1638 (1992).
- <sup>44</sup>D. G. Schweitzer, *Phys. Rev.* **128**, 556 (1962).
- <sup>45</sup>R. Siegele, J. Roth, and B. M. U. Scherzer, *J. Appl. Phys.* **73**, 2225 (1993).
- <sup>46</sup>G. Ramos and B. M. U. Scherzer, *Nucl. Instrum. Methods B* **85**, 479 (1994).
- <sup>47</sup>T. Iwata, F. E. Fujita, and H. Suzuki, *J. Phys. Soc. Jpn.* **16**, 197 (1961).
- <sup>48</sup>T. Tanabe, T. Maruyama, M. Iseki, K. Niwase, and H. Atsumi, *Fusion Eng. Des.* **29**, 428 (1995).
- <sup>49</sup>P. Goggin and W. N. Reynolds, *Philos. Mag.* **8**, 265 (1963).